J. Fluid Mech. (1972), *vol.* 52, *part* 1, *pp.* 137–160
Printed in Great Britain

An experimental study of the velocity distribution and transition to turbulence in the aorta

By R. M. NEREM,† W. A. SEED AND N. B. WOOD‡
Physiological Flow Studies Unit, Imperial College, London

(Received 29 September 1971)

The development and evaluation of a hot-film probe, suitable for use within arteries and operated with a commercial constant-temperature anemometer and linearizer, is described. The performance of the system in the recording of arterial velocity wave forms is described, and instantaneous and time-averaged velocity profiles constructed from measurements in the thoracic aorta of dogs are presented. The profiles were blunt, with boundary layers estimated to be less than 2 mm thick throughout the cycle, and significant skews were observed, the explanation for which appears to lie in the influence of local geometry on the flow. A preliminary study of flow disturbances in the aorta based on visual observation of instantaneous velocity wave forms and frequency spectrum analysis is reported. The occurrence of flow disturbances and turbulence is shown to be related to peak Reynolds number and the frequency parameter α. The possible roles of free-stream disturbances and boundary-layer transition in generating these disturbances are discussed.

1. Introduction

The analysis of flow in major mammalian arteries presents a number of fluid-dynamical problems since the flow is pulsatile, commonly with a reversing phase, and passes through vessels of complex geometry. Whilst techniques to measure pressure and flow in such systems have been available for some time, point velocity measurements had not previously been achieved and the complexity of the system has severely inhibited theoretical evaluation and model studies.

Recently, reports of the use of constant-temperature hot-film anemometer systems for such measurements have begun to appear in the physiological literature. Seed & Wood (1970*a*, *b*) have discussed the problems associated with the use of hot-film anemometry in the arterial environment and described the development of a suitable system. This system has been used in the aorta to measure velocity profiles, and in a preliminary study of the generation of turbulence. This paper presents some features of general fluid-dynamical interest which emerged both in the development of the instrument and from the results of the physiological studies.

† Present address: Department of Aeronautical and Astronautical Engineering, The Ohio State University.
‡ Present address: The Central Electricity Research Laboratories, Leatherhead, Surrey.

2. General considerations

The aorta (figure 1, plate 1) is the main artery supplying oxygenated blood to body tissues via its branches. It is fed through the aortic valve from the left ventricle of the heart. At its origin it is directed towards the head (ascending aorta), but within about three diameters it arches through 180°, with major branches leaving it at 90°, and runs along the spine towards the abdomen as the descending aorta. It is tapered, with an initial diameter up to about 2 cm in the dog (a common experimental animal).

Flow into the aorta is pulsatile, with each ventricular contraction producing a short period of forward flow (systole) characterized by rapid acceleration to velocities of 100–200 cm/s followed by deceleration, and with valve-closure being associated with a period of flow-reversal and marking the onset of diastole. The time-mean component of the velocity varies between approximately 5 and 30 cm/s.

It is commonly assumed that the velocity distribution at the entrance to the aorta is uniform. However, it has not been possible until recently to check the assumption experimentally and it is not known what influence the pattern of ventricular contraction will have. Furthermore, the cusps of the aortic valve lie just inside the entrance, although, experiments in a model of the aortic valve region by Bellhouse & Talbot (1969) have suggested that disturbances from this source should be slight. In another model representing the atrium and ventricle, Bellhouse (1970) found that a vortex is formed in the ventricle during filling from the atrium as a result of the flow through the mitral valve. This is likely to persist into the ventricular contraction phase, with a corresponding influence on the aortic entrance flow.

Although steady flow patterns in the entrance region of straight rigid pipes are known (Nikuradse 1934), the modifying effects of unsteady flow and elastic boundaries make it difficult to predict what will happen except perhaps in the ascending aorta, where a number of studies (Atabek & Chang 1961; Kuchar & Ostrach 1967; Jones 1970) suggest that there will be an inviscid core with a thin aortic wall boundary layer. In the arch the situation becomes more complicated; flow entering a bend will develop an asymmetric velocity profile. In a fully developed viscous flow the higher velocities are on the outside of the bend, as a result of the action of secondary motion (Goldstein 1938). In inviscid flow with a flat entry profile there is no secondary motion and the higher velocities develop near the inner wall (Seed & Wood 1971). Since the form of the boundary layer in the arch is uncertain, it is difficult to predict the magnitude of its influence. Furthermore, the presence of two large branches must exert an influence, both geometrically and by their effect on wave transmission and reflexion.

With regard to the extent to which flow disturbances and/or the development of turbulence may occur within the normal circulation, very little information exists in the literature. In general, engineering studies have examined turbulence and the transition from laminar to turbulent flow primarily in steady flows. However, the problem in arteries has been uniquely difficult, partly because of the unsteady nature of the basic flow and partly because of the limitations of

instrumentation and access. As an example, the standard techniques for demonstrating the onset of turbulence in a pipe flow – the breakdown of the Poiseuille pressure–flow relationship, or direct flow visualization – are inapplicable or difficult to apply in unsteady flow. Because of this, discussion of the onset of turbulence in arteries has been largely speculative and based on comparison with the behaviour of steady flow regimes. Such speculation has suggested that turbulence might occur in larger arteries during systole. (Using the figures quoted earlier, the mean pipe Reynolds numbers lie between 250 and 1500, but peak Reynolds numbers are of the order of 5000.) The few attempts which appear to have been made to examine arterial flow *in vivo*, either by direct cinematography of injected dye (McDonald 1960) or by cineradiography (Ohlsson 1962), have tended to bear this out.

There have been a limited number of studies of the stability of pulsating pipe flows (Yellin 1966; Sarpkaya 1966) and these have centred primarily around the growth and decay of disturbances in sinusoidally accelerating and decelerating flows. Unfortunately, the experiments have been carried out for α values of 4–6, which are somewhat lower than those encountered in aortic flows, and for conditions where the oscillatory component was small compared with the mean. Because of the low α values, the side-wall boundary layer is somewhat thicker than that in the aorta and the flow might even be fully viscous. The small oscillatory components, on the other hand, correspond to domination of transition by the mean flow properties.

It is these features of arterial flow which indicate the primary requirements for an arterial hot-film probe. From a practical viewpoint this probe should be suitably shaped for insertion and must be small and robust. In addition, since the hot-film system does not intrinsically distinguish forward from backward flow, some auxiliary means of signalling flow reversal must be provided. Furthermore, Fourier analysis of records from electromagnetic flow meters (which give a fairly accurate instantaneous cross-sectional mean velocity) shows that harmonics of the heart rate up to about the tenth may have significant amplitude. The fundamental frequency in dogs is 1–3 Hz, thus the overall system should have a frequency response which is flat to at least 25 Hz to reproduce the velocity wave form. However, identification of flow disturbances and turbulence will necessitate a response at frequencies up to several hundred hertz.

The probe must also be capable of operating in a conducting fluid, since blood contains a number of ionic constituents, and the overheat must be limited to less than 10 °C to prevent deposition of heat-sensitive blood constituents on the film. Finally, a calibration apparatus which provides known water or blood flows, both steady and oscillatory, over the range 0–100 cm/s is needed. It must also include facilities for maintaining blood at 37 °C and should preferably require only small volumes.

3. Anemometer system *Anemometers*

Commercially available circuits have been used throughout this work. The results described here were obtained with a DISA 55 D01 anemometer and DISA 55 D10

linearizer. The anemometer was modified by incorporation of an additional series resistance decade to allow balancing to 0·001 rather than 0·01 Ω and by the insertion of a switched resistor in parallel with the upper arm of the bridge. The value of this was chosen as 1 % of the arm so that when switched in it provided 1% overheat automatically; with the gold films used, this gave a 5 °C overheat.

Probes

Laboratory fabrication techniques have been described by Seed (1969) and some of the design considerations for such probes were discussed by Seed & Wood 1970*a*. The most satisfactory solution has been to limit the size and to use a flow splitting shape with films at near zero incidence on a flat or only very slightly curved surface. The probe shown in figure 2 has proved the most satisfactory design to date since the small surface curvature prevents flow separation throughout the wide range of Reynolds numbers that occur within arteries. Three gold

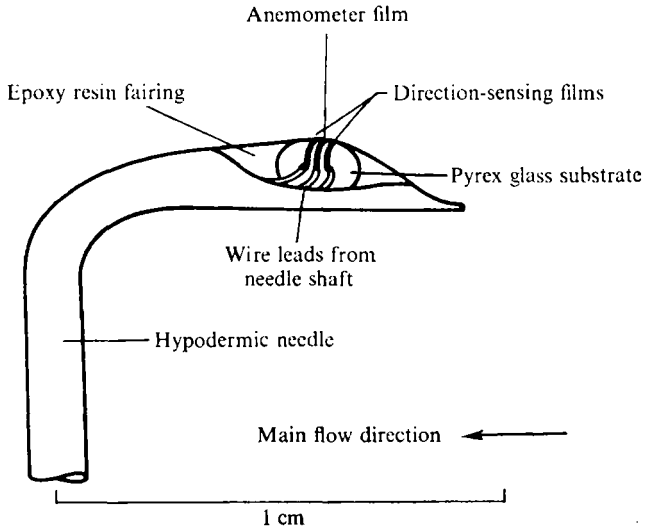

FIGURE 2. Intra-arterial velocity probe.

films, each 0·2 × 0·5 mm, are set side by side, about 0·1 mm apart and at right angles to the flow axis, on the surface of a Pyrex bead which is then mounted on a hypodermic needle (0·75–1·5 mm O.D.) whose tip has been built up and faired with epoxy resin to the desired shape.

Each film is electrically independent. The central film is connected to the anemometer and used for measurement of flow velocity; the other two are used to signal flow direction. In steady flow such probes yield stable signals provided precautions are taken to avoid film damage and to allow for temperature variations in the liquid. The latter is a minor problem since resetting of the overheat ratio is a simple and rapid manoeuvre. Protecting the films permanently from damage, particularly electrolytic etching, is best achieved by coating the film with silicon resinate during construction of the probe, using the technique described by Vidal & Golian (1967). The thickness of the layer obtained is of the order of 1 micron and has a negligible effect on the frequency response.

Direction sensing

Films placed on either side of and close to the heated film, and connected as two arms of a Wheatstone bridge, were found to give an unequivocal indication of flow direction. They act as resistance thermometers, registering the bias in streamwise temperature distribution in the substrata caused by the flow and exhibiting only slight velocity sensitivity. The bridge unbalance signal changes polarity with flow direction change and can be used to generate pulses in a comparator circuit. These pulses will switch polarity in a compatible unity-gain switched amplifier which carries the velocity signal. Thus the part of the (rectified) velocity signal which corresponds to reverse flow can be automatically inverted before display.

4. Calibration

Direct method

Steady velocities were generated by rotating liquid in an annular channel in a circular vessel on a gramophone turn-table (Seed & Wood 1969). Probes were clamped above the dish and lowered into the liquid. The system allows calibration in small steps up to 120 cm/s, using 150 ml of liquid. The temperature of the liquid can be held constant by circulating water (from a thermostatically controlled heater circulator) through the spaces either side of the channel in the dish. The validity of the system was checked by a comparison of signals obtained in a towing tank and on the turn-table, using the same probe.

Unsteady velocities were generated by mounting the probe in a mechanical oscillator which produced simple harmonic motion at frequencies up to 15 Hz. The probe could therefore be exposed to sinusoidal fluctuations of velocity in still liquid, or with any desired mean flow. The method of calibrating probes by oscillation in still fluid (Schultz *et al.* 1969) is attractive because of its simplicity, but was shown to be subject to artefacts caused by secondary flow generation (Seed & Wood 1970*a*).

Indirect method

The frequency response of the constant-temperature system in its operating mode was examined by coupling an oscillator across the film and injecting a sinusoidal voltage under the conditions recommended for the square-wave test (DISA 55 D01 anemometer handbook). The injection of an electrical signal has disadvantages as a method of calibrating the instrument, particularly at low frequencies, since the temperature distribution in the film should be nearly uniform, requiring that conduction in the substrata should be approximately one-dimensional. This is more likely for a depth of penetration $(k/\omega)^{\frac{1}{2}}$ of thermal waves into the substrata small compared with the smallest film dimension. On this basis the method should be valid for frequencies down to 2–3 Hz.

In fact, the frequency response measured electrically, which gives an indication of both the anemometer behaviour and the effect of thermal conduction in the substrata, has been found to reflect closely that inferred from direct flow calibrations. The method has been found valuable in comparing the response

characteristics of different constant-temperature circuits and overheat settings and in monitoring the effect of necessary modifications.

5. System performance

Steady flow

Calibrations in both blood and water with these probes have been found to fit the anemometer equation

$$V^2 = A + Bu^n, \tag{1}$$

using V_0^2 (where V_0 is zero flow voltage) in place of A, and a value of $\frac{1}{2}$ for the velocity exponent n. (B is a constant depending on the fluid properties, the probe body shape and dimensions, the anemometer bridge ratio and the temperature difference between film and environment, dictated by the overheat ratio.) Serial calibrations with a single probe over a period of weeks were normally repeatable within $\pm 5\,\%$.

Comparison between calibrations performed with the same probe at the same overheat in blood and water revealed differences in the term A, but not in B. Heat-transfer theory for homogeneous fluids predicts a difference in term B because of differences between the bulk fluid properties of blood and water. The cause of this discrepancy has been discussed previously (Seed & Wood 1970*b*) and is ascribed to the inhomogencity of blood.

Frequency response

Both electrical and oscillatory flow calibrations revealed that the anemometer showed a rising frequency response when operated with these probes at 1 % overheat ratio. It proved possible to improve the frequency response with a single stage output filter (Seed & Wood 1970*b*). The response remains velocity-dependent but can be made flat within $\pm 10\,\%$ from d.c. to 400 Hz for velocities within the physiological range.

However, the boundary layer generated by the flow over the probe also governs heat transfer from the film and requires a finite time, which is dependent on flow velocity, to reach a steady state. This modifies the behaviour in unsteady flow and is likely to appear as an error in the registration of rapidly changing velocities near zero. It can be characterized (Seed & Wood 1970*b*) in terms of the non-dimensional parameter fx/u, where f is the frequency, x is the distance along the probe from leading edge to the film (boundary-layer length) and u is the instantaneous velocity.

Thus the probe should be physically small to minimize x, but there still remain times in the arterial velocity cycle when u falls to zero, leading to progressively larger proportional errors. Oscillatory calibration studies in reversing flows have suggested that backward velocities will be registered to within $\pm 20\,\%$ in the range of velocity and frequency encountered within arteries. The establishment of equal sensitivity to forward and backward components of unsteady reversing flows has proved the most difficult feature of probe design; Seed & Wood (1970*b*) and Wood (1971) have discussed the subject in detail. Figure 3 shows steady and unsteady probe calibrations performed in blood at 37 °C.

In summary, the calibration studies have demonstrated that the major part of the systolic velocity wave form can be measured within ± 5 % (calibration accuracy). At low velocity and during flow reversal, errors occur which are large proportionally but small in absolute terms (probably always less than 5 cm/s). During reverse-flow phases of the cycle accuracy limits are looser (± 20 %).

The calibrations described were performed in unsheared flows. To investigate

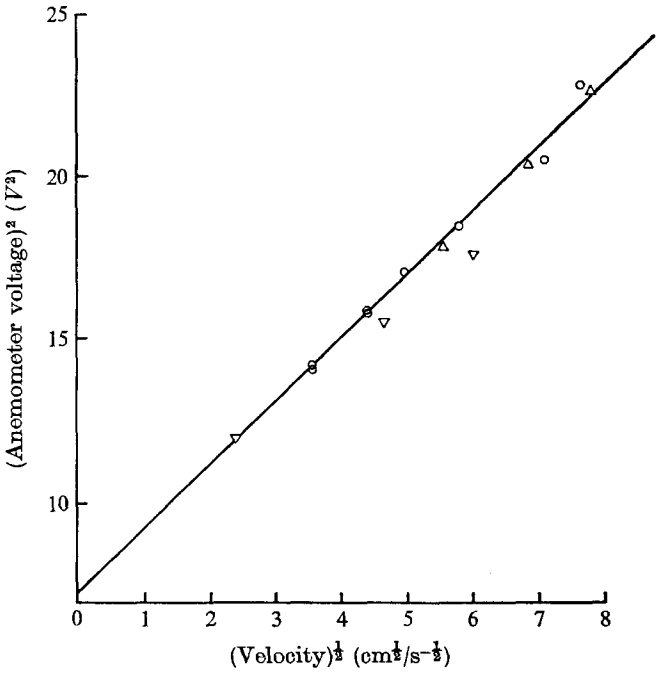

FIGURE 3. Static and dynamic calibrations of probe in blood at 37 °C, numerically linearized as square of signal against square root of velocity. ○, steady flow. Oscillation at 3 frequencies in steady flow of 13 cm/s: △, peak forward velocity; ▽, peak backward velocity.

the probe response in a velocity gradient, traverses were made of steady pipe flow both near the entrance and in the fully developed region. These showed that the probe measured the velocity of the streamline approximately midway between the probe tip and the film position, and that as expected, because the film was mounted on a projection ahead of the shaft, blockage effects were negligible.

6. Methods

The experiments were performed on dogs under general anaesthesia. At the beginning of each experiment, the probe was calibrated in steady flows of blood taken from the animal and maintained at 37 °C in the turn-table apparatus. Before the calibration, the system frequency response was adjusted via the output filter, using the electrical test described earlier. At the same time, the Wheatstone bridge containing the twin direction-sensing films was balanced to give zero volts at zero flow. All outputs were recorded on magnetic tape with a

multichannel FM recorder (Precision Instruments PI-6200). Figure 4 shows a typical velocity calibration. The aorta was exposed surgically. The probe was inserted by direct puncture, aligned on a diameter normal to the vessel and clipped into the slide of a graduated plastic carrier to allow traversing across the vessel.

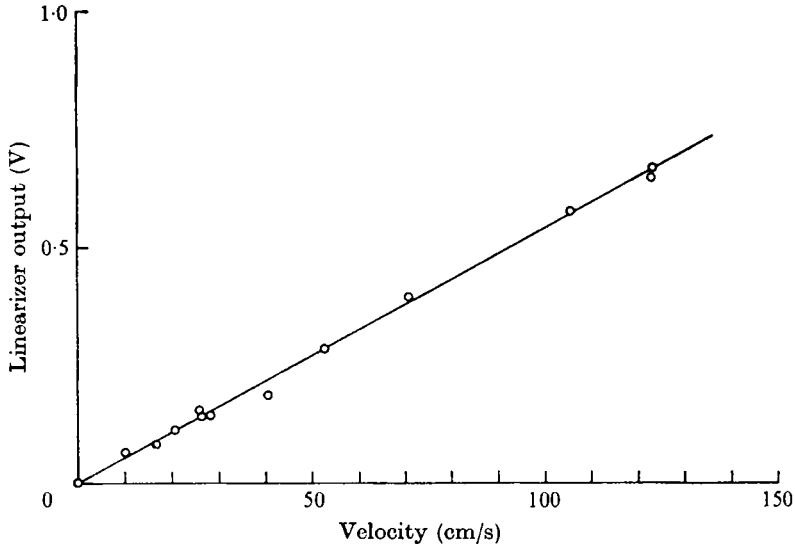

FIGURE 4. Steady flow calibration of probe in blood at 37 °C linearized with DISA 55 D10 linearizer.

The general object of the experiments was to record velocity wave forms in small steps across the vessel and to use these for reconstruction of instantaneous and time-averaged velocity profiles. Since both heart output and downstream flow-resistance are subject to reflex control; variation in local flow conditions may occur within an artery both gradually and beat-to-beat. Traverses were therefore carried out in pairs, inward and outward, so that slow changes would be identifiable as opposite skewing of the profiles. In addition, records were usually taken repeatedly at a single reference station on the diameter during at least one traverse. Beat-to-beat variation was eliminated by averaging; at playback, the velocity signals from each recording station were played into an averaging oscilloscope (Northern Instruments NS-513) which was triggered to sweep one or two beats by the ECG signal, which immediately precedes the flow events. The averaged wave form was then played out onto a pen recorder at the end of each run of beats. Each traverse was thus reduced to a set of averaged velocity wave forms, one for each recording station, which were measured at chosen intervals through the cycle in the reconstruction of instantaneous velocity profiles. A fairly typical wave form, recorded in the ascending aorta and averaged as described, is shown in figure 5. Time-averaged velocity profiles were obtained by replaying the velocity signals from each traverse station through an electronic integrator.

Individual wave forms were also examined during each experiment for evidence of flow disturbances or turbulence. In addition, experiments were performed in

which peak Reynolds numbers and heart rate were varied, together or separately, by drugs and other manoeuvres, whilst velocity was recorded with a probe on the centre-line of the vessel. The velocity signals were passed through a frequency spectrum analyser (Brüel & Kjaer Audio frequency Spectrometer Type 2112), whose output was recorded on an ultra-violet paper recorder with 450 Hz

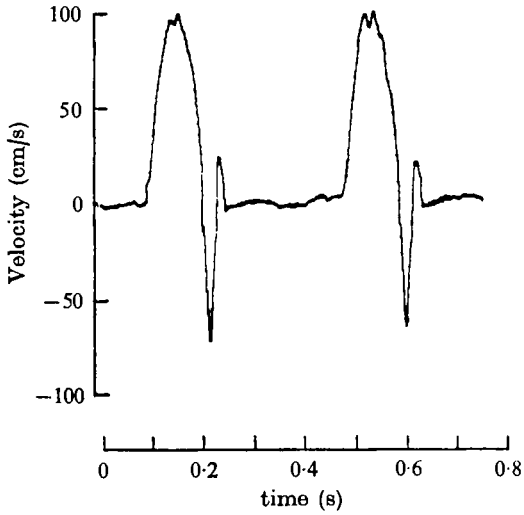

FIGURE 5. Instantaneous velocity wave form in ascending aorta averaged from many beats as described in the text.

galvanometers. The spectrum analyser allowed instantaneous analysis in $\frac{1}{3}$ octave steps and gave an output which represented the instantaneous peak-to-peak amplitude of velocity fluctuations within a $\frac{1}{3}$ octave band about the set centre frequency.

It should be noted that the quantitative description of flow disturbances, even by spectral analysis, is somewhat unsatisfactory where the basic flow is unsteady, since the spectra combine the harmonics of the unsteady flow with any random high frequency components representing turbulence. Individual spectra obtained under different conditions can, however, be rendered more readily comparable if they are normalized in terms of heart rate and it is then possible to demonstrate relative changes in energy content, where they occur, and check impressions gained by visual inspection of velocity wave forms. A more sophisticated analysis of spectral energy content, incorporating other parameters such as boundary-layer thickness and the scale of disturbances, was not used at this stage since the origin and structure of arterial flow disturbances have not previously been investigated.

7. Results and discussion

Velocity distribution

Representative velocity profiles derived from the averaged wave forms are shown in figure 6. Antero–posterior traverses of the ascending aorta are given in figures

6(*a*), (*b*) and (*c*) from the lower, middle and upper sites respectively. Figure 6(*d*) shows a left–right traverse at the upper site. In each case, five phases in the cycle deduced from the averaged wave forms are displayed on the left of the

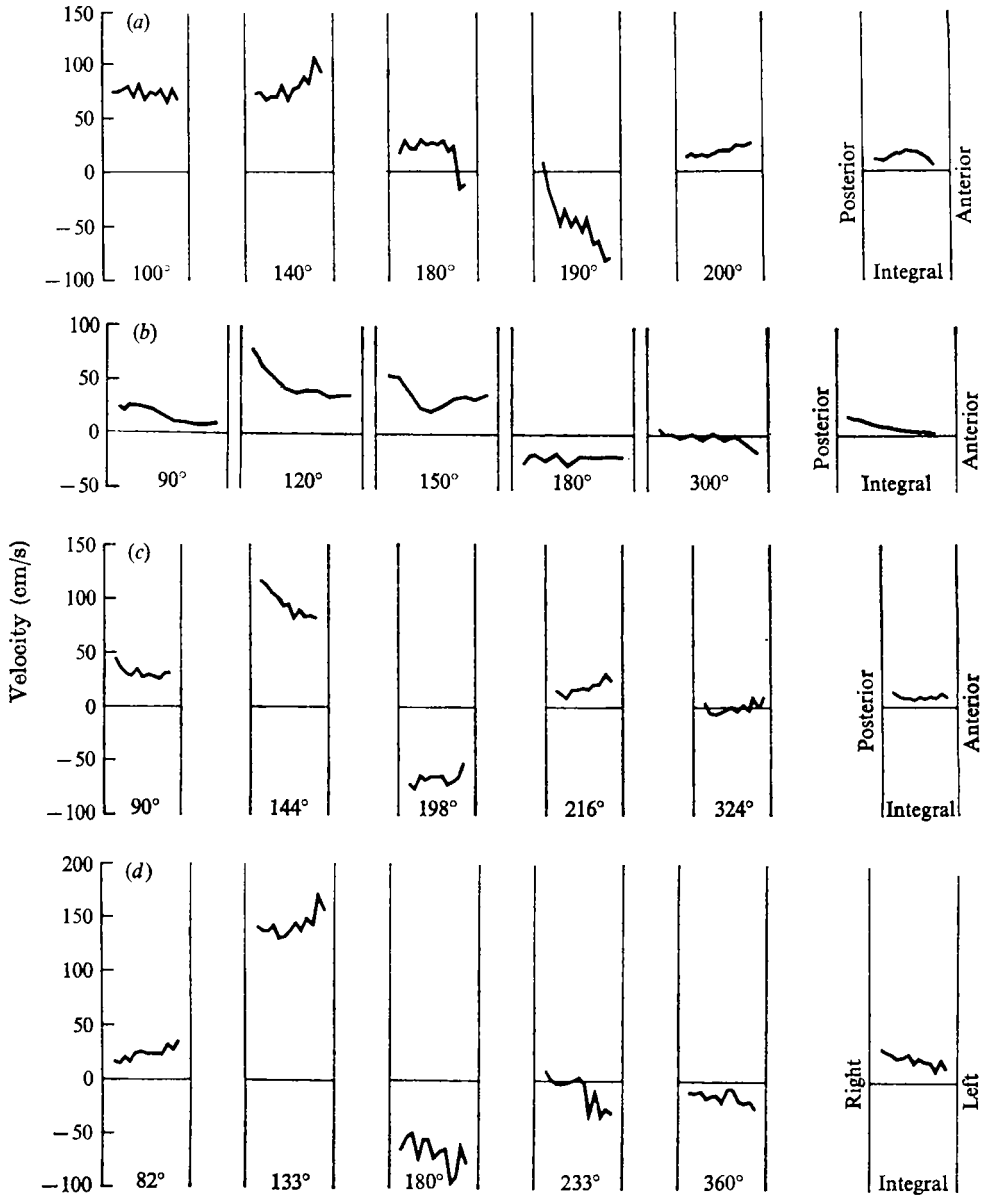

FIGURE 6. Velocity profiles in ascending aorta, constructed from averaged beats (see text). The origin (0°) is in all cases the R wave of the ECG. Time-averaged profiles for each site appear on the right. (*a*) Lower site (approximately 1 cm from aortic valve), antero–posterior traverse, diameter 16 mm, pulse rate 194/min. (*b*) Middle site (2 cm from aortic valve), antero–posterior traverse, diameter 22 mm, pulse 163. (*c*) Upper site (3 cm from aortic valve), antero–posterior traverse, diameter 14 mm, pulse 194. (*d*) Upper site, left–right traverse, diameter 16 mm, pulse 190.

figure; the profiles on the right are the time-averaged results. Points closer than 2 mm from the walls have been deliberately excluded, because the probe distorts the profile at the near wall (as shown in the pipe tests mentioned earlier), and because the vessel was unrestrained at the far wall. The thoracic aorta expands

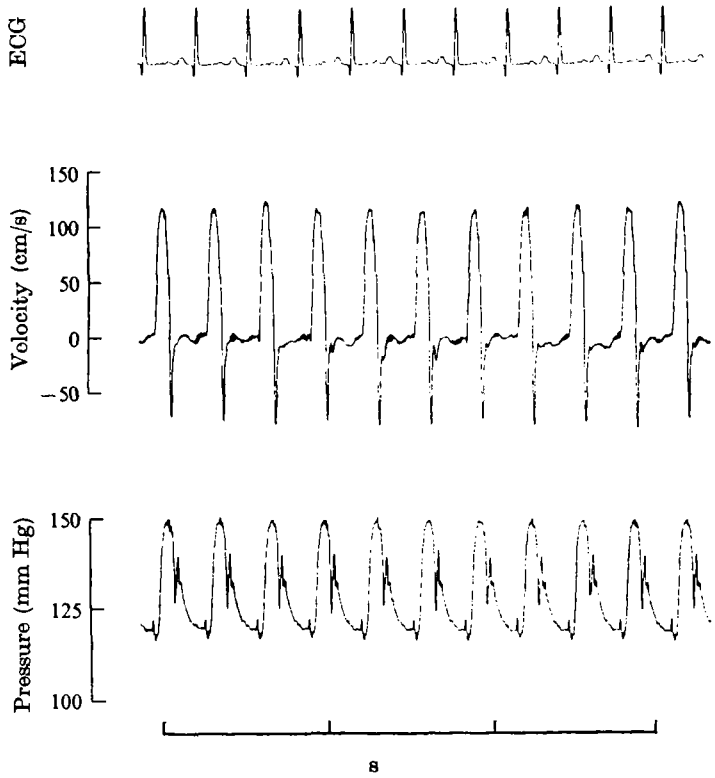

FIGURE 7. Simultaneous record of ECG, centre-line velocity in ascending aorta and aortic pressure.

and contracts radially by approximately 7 % with each pulse (Barnett, Mallos & Shapiro 1961). Whilst the peak radial wall velocities associated with this were estimated to be only 3–7 cm/s in the present experiments, the proportional errors in radial position relative to the wall are larger the closer the approach to the wall.

The range of peak systolic velocities measured at the axis of the ascending aorta is of the same order as would be expected from the observed pressure. For the inviscid core, neglecting effects of wave reflexion, the equation of motion may be approximated by

$$\frac{\partial u}{\partial t} = -\frac{1}{\rho}\cdot\frac{\partial p}{\partial x} = \frac{1}{\rho c}\cdot\frac{\partial p}{\partial t}, \tag{2}$$

so that pressure and velocity are in phase, as can be seen in figure 7. Of course, at other points in the cycle the inviscid relationships breaks down because of both viscous effects and wall movements. The peak systolic velocity will be approximately $\Delta p/\rho c$, where Δp is the pulse pressure (the difference between systolic and diastolic pressure). In figure 7, $\Delta p \simeq 35$ mm Hg and, taking $c = 500$ cm/s in the

thoracic aorta (McDonald 1960), this gives a peak systolic velocity of nearly 100 cm/s, which is close to that measured.

Looking first at the instantaneous velocity profiles, the feature which is most striking is the presence of skews in the majority of cases, even at the lower site close to the entrance of the aorta. For the antero–posterior traverses the explanation of the behaviour at the site nearest the heart is least clear. In early systole (100°) the velocity is uniform, whereas later (140°) a pronounced asymmetry is seen, with higher velocity towards the anterior wall. This is associated with marked disturbances in the velocity wave form as shown in figure 8.

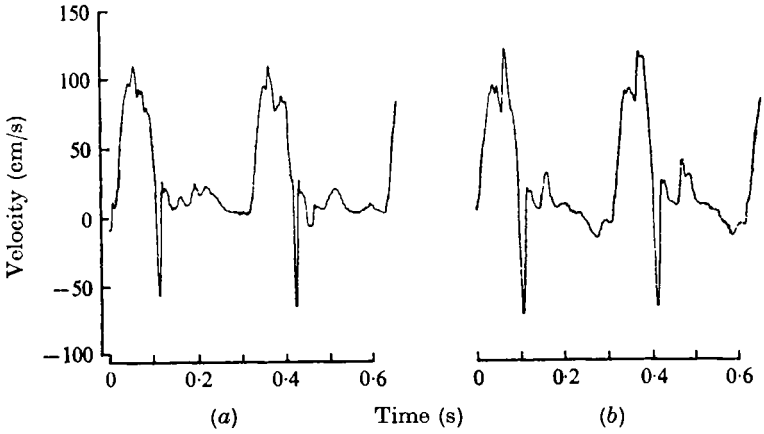

FIGURE 8. Individual velocity wave forms in lower ascending aorta, (*a*) posterior, (*b*) anterior.

The disturbances were present on each wave form and were not eliminated by averaging, thus indicating that they contained a major component in phase with the fundamental wave form such as the vortex which forms in the ventricle during filling or disturbances originating around the cusps of the aortic valve. At this site, disturbances were a normal observation and scatter in the reconstructed velocity profiles, despite averaging, was in general greater than at other sites. Such disturbances clearly have a strong influence on the detailed form of the velocity profile during systole. If they are generated from one of the origins suggested, variation from animal to animal, related to the pattern of ventricular contraction or orientation of the probe to the valve cusps, is to be expected. Furthermore, the disturbances may mask other factors operating to generate skews in the profile. For example, the axis of the ventricle lies at an angle to that of the ascending aorta and inviscid flow in such a bend would have an asymmetrical profile of the form observed. It is not clear whether the disturbances are the sole cause of the skew in late systole or obscure a skew which would otherwise be observed in early systole.

The early diastolic skew at this site (190°) could also originate from inviscid flow through the bend but its orientation is consistent with drainage to the coronary arteries. The major proportion of coronary flow, which is typically 5–10 % of the flow leaving the ventricle, occurs during diastole and, as seen in

figure 1 (plate 1), the coronary arteries originate near the anterior and left-posterior walls.

These skews are not maintained as blood travels up the ascending aorta. At the upper site, the prominent feature throughout forward flow is an opposite skew, with higher velocities near the posterior wall (figure 6(*c*)). At the middle site (figure 6(*b*)) both lower and upper influences act, causing an inflected profile as velocities fall in late systole. The upper site is just into the bend of the arch and its profiles strongly suggest inviscid behaviour in the broad core of the flow, under the influence of a centrifugal pressure gradient as mentioned in § 2. When flow reverses (144–198°) the profile becomes a mirror image under the same influence. Thereafter, the effect breaks down; when the second direction change occurs (216°) the profile behaves as if only a uniform axial pressure gradient were acting.

There are several factors which might explain this feature. One is that Reynolds numbers are much lower; thus viscous forces might inhibit the centrifugal effect, so that there is insufficient time for the skew to re-establish. This explanation is supported by an axisymmetric velocity profile observed in very early systole (not shown) when the Reynolds numbers were similar. Alternatively, or additionally, the pattern of flow near the aortic arch branches may be relevant. Certainly during late diastole (234° onwards) anterior forward flow and posterior backward flow is maintained, suggesting a circulating flow. No measurements were made in the branches leaving the aortic arch during these experiments but the evidence from electromagnetic flow meter measurements (see, for example, Inouye & Kosaka 1959) is that forward flow may be maintained in these vessels during diastole. In addition, the impedance offered to the streamlines entering the branches is probably different from that experienced by the flow which continues around the aortic arch. Furthermore, there appear to be quite significant pressure wave reflexions from the junctions in the arch as may be inferred from the change in pressure wave form from the lower to the upper ascending aorta shown by Noble, Gabe, Trenchard & Guz (1967). The possibility also exists that close to the junctions (within approximately one diameter) the reflected component of the pressure wave is not uniform across the vessel.

It has been confirmed that the skews measured at this site were not an artefact due to progressive changes in flow alignment across the vessel relative to the probe, by use of a probe which was insensitive to flow direction in the plane of the traverse. It has not, however, been established whether a secondary motion component was present in the measurement. The traverse which is shown for the left–right plane at this level (figure 6(*d*)) is slightly skewed throughout, with higher velocities along the left wall. In the aortic cast, which is of course from a different dog, there is slight curvature in this plane which would explain the effect but in another animal the skew was absent. Again local geometry is likely to be important. Although traverses in the left–right plane were not possible nearer to the heart because the pulmonary artery overlies the aorta, some idea of the three-dimensional flow changes which occur through the cycle in that region can be obtained from a comparison of figures 6(*c*) and (*d*).

In summary, these profiles tend to confirm that during most of systole a broad inviscid core exists, as discussed in § 2, and dominates the flow. The integrated

profiles, which represent the time-mean flow velocities, are blunt, with the exception of the site nearest the heart. This latter was the site where low frequency, i.e. large-scale, disturbances were present in the velocity wave forms which would be expected to have an effect on the mean component. Further away from the valve, where the disturbances had damped in the experiments in which velocity profiles were examined, the mean flow profiles were blunt.

Turbulence studies

Visual examination of individual wave forms during these experiments suggested that wave forms should be divided into three types, which are shown in figure 9. Those with negligible high frequency components (figure 9(*a*)) are termed

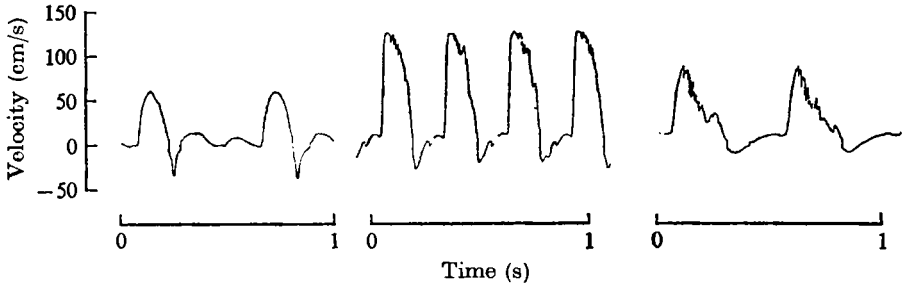

FIGURE 9. Velocity wave forms recorded in descending thoracic aorta, (*a*) undisturbed, (*b*) disturbed, (*c*) highly disturbed.

undisturbed and are representative of laminar flow. Those with high frequency components present only at the peak systolic velocity (figure 9(*b*)) are termed disturbed and are thought to represent a transitional condition. Those with high frequency components persisting throughout the deceleration phase of systole are termed highly disturbed and are thought to be representative of turbulence (figure 9(*c*)). This division is of course qualitative, though it was rarely difficult to categorize a wave form. Frequency analysis of the disturbed and highly disturbed wave forms showed appreciable amplitudes of the high frequency components during systole, with what appeared to be random fluctuation from beat to beat. A feature, which was very obvious on the output signals from the spectral analyzer and is also clearly seen in figure 9, is that disturbances are confined to systole and are damped out during diastole. The fact that they appear again on the following beat indicates that they are generated anew on each beat.

Figures 10–12 present a number of examples of the measured distribution of kinetic energy over the frequency spectrum covered. The spectrum of turbulence may be characterized by a distribution function $F(n)$, where n is frequency (Schlichting 1968). The function $F(n)$ represents the non-dimensional distribution of kinetic energy as a function of frequency such that

$$\int_0^\infty F(n)dn = 1. \tag{3}$$

In the plots presented here, a modified non-dimensional spectral energy distribution has been presented, i.e.

$$F_1(n) = \frac{\overline{u_n'^2}}{\hat{u}^2 . \Delta(n/n_1)}, \tag{4}$$

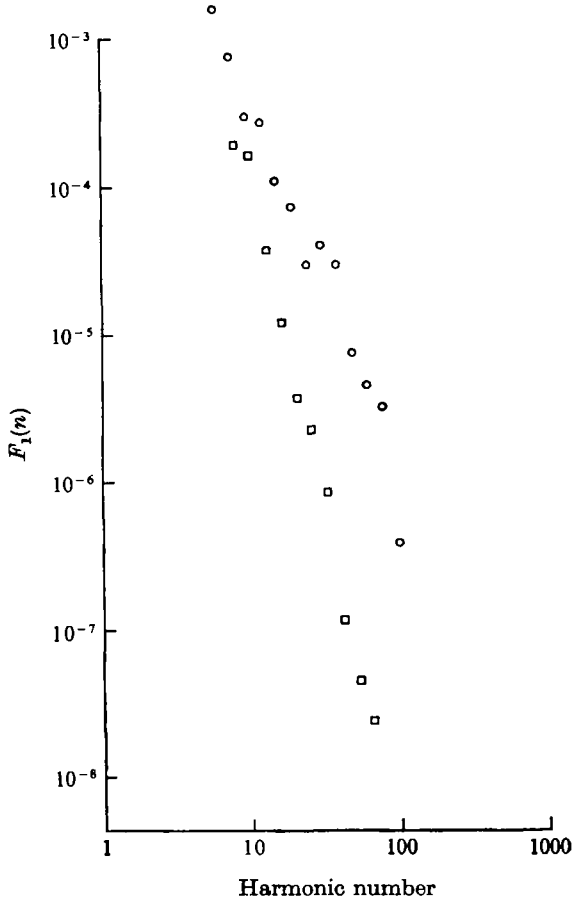

FIGURE 10. Power spectra for high frequency components of aortic flow: non-dimensional spectral energy density versus harmonic of heart rate. Same animal, descending aorta; □, control; O, isoprenaline infusion.

where $\overline{u_n'^2}$ is the mean-square value of the fluctuating velocity based on a sample average of the signals for each frequency band with centre frequency n and bandwidth Δn, $\hat{u}$ is the peak systolic velocity and n_1 is the heart rate (i.e. the fundamental harmonic frequency). The data are presented as a function of harmonic number rather than frequency to facilitate comparison between spectra obtained in different animals or at different heart rates in the same animal. Thus the abscissae in figures 10–12 are harmonics of the heart rate and the ordinates are the fractional systolic energy distribution per harmonic.

In figure 10 spectra are shown for an undisturbed and a highly disturbed wave form in the descending aorta (isoprenaline is a powerful cardiac stimulant). It

should be noted that the basic wave form of an aortic flow can normally be described using approximately 10 harmonics. For the undisturbed case in figure 10 only 0·01 % of the energy is represented at higher harmonics; for the highly disturbed case the figure is 0·25 %. The maximum separation from the undisturbed spectrum occurred at 100–150 Hz, which agrees well with the estimates

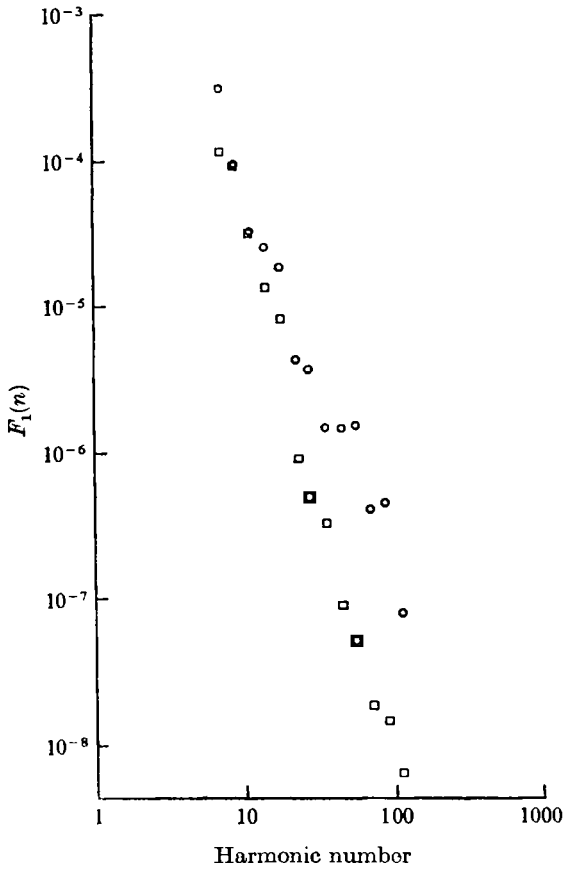

FIGURE 11. Power spectra, as in figure 10. Same animal, isoprenaline infusion; ○, aortic arch; □, descending aorta.

based on vessel diameter and peak velocity. It was thus of interest to attempt to define the origin of the disturbances, in the sense of distinguishing between free-stream turbulence existing in the blood ejected from the ventricle, and boundary-layer transition in the aorta itself. Using time-averaged velocities, and assuming blunt velocity profiles, we find that blood ejected from the heart reaches the arch region during one beat and penetrates the descending aorta on the second beat, after a diastolic period.

In figure 11 spectra for similar conditions of flow in another animal are shown in both the arch and the descending aorta. The high frequency content in the arch is considerably increased over that in the descending aorta and tends to implicate flow disturbances originating in the ventricle as origins of turbulence.

In figure 12, however, spectra from the ascending and descending aorta are presented under two conditions of flow. In the first ('resting') case disturbances are again present in the ascending aorta, while flow in the descending aorta is undisturbed. In the second (after administration of isoprenaline) the second beat flow in the descending aorta became highly disturbed. In all these cases diastole was a quiescent period, and the disturbances in the descending aorta appear not to have been convected from the heart but locally generated.

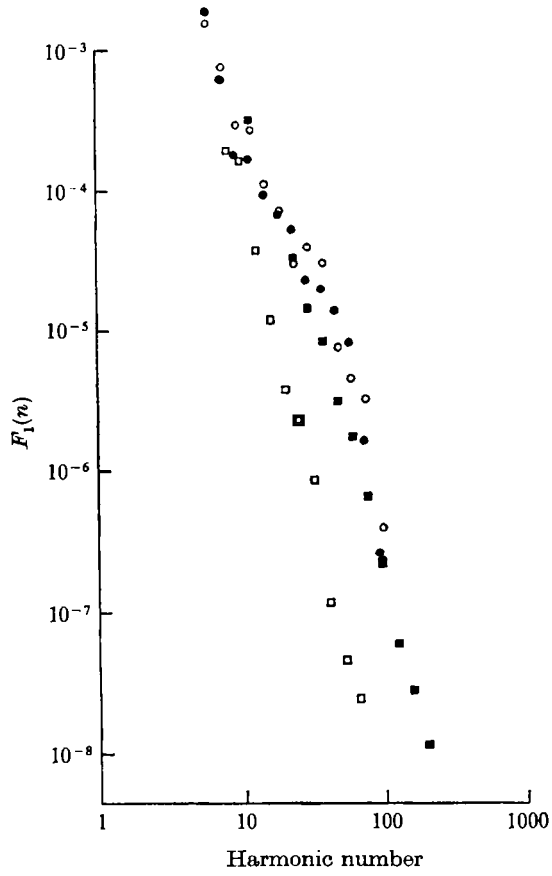

FIGURE 12. Power spectra, as in figure 10. Same animal. Ascending aorta: ■, control; ●, isoprenaline infusion. Descending aorta: □, control; ○, isoprenaline infusion.

During the experiments on velocity distribution described earlier, it became clear that the appearance of disturbed or turbulent wave forms could not be explained solely on the basis of peak Reynolds number ($\hat{R}e$), but that heart rate appeared to be implicated. The other groups reporting arterial measurement with hot-film systems (Schultz *et al.* 1969; Ling *et al.* 1968) have both observed that turbulence was an occasional phenomenon occurring in smaller animals only. These observations suggested that the parameter α might have significance, since it incorporates terms proportional to both vessel size and heart rate. In figure 13 the data for the descending aorta are summarized in terms of $\hat{R}e$, α and

the extent of the disturbances observed. As indicated in the figure, the shaded points represent highly disturbed or turbulent conditions, the half-shaded points represent disturbed conditions and the open points undisturbed or laminar conditions. Furthermore, points obtained in the same animal under different conditions are connected by a straight line.

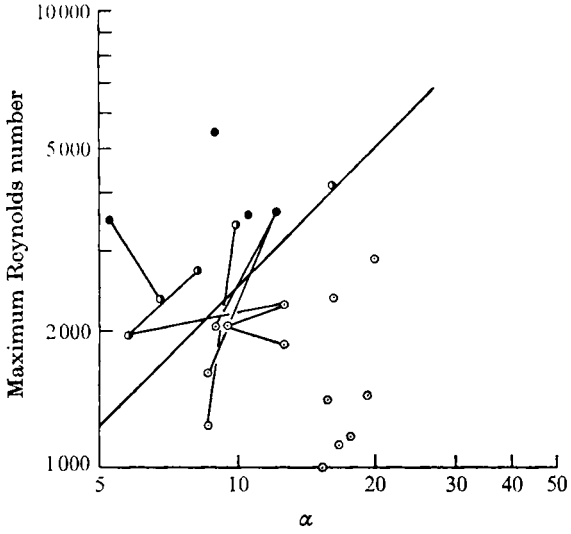

FIGURE 13. Reynolds number and frequency parameter α for the descending thoracic aorta. ○, undisturbed flow; ◑, disturbed flow; ●, highly disturbed flow; ——, equation (5).

Although there are a number of points where for a variety of reasons only one flow condition was observed, there seems to be in all this data a general trend whereby increasing $\hat{R}e$ and/or decreasing α leads to a more disturbed flow condition, and the demarcation between undisturbed and disturbed or highly disturbed conditions seems to approximately follow a line having the equation

$$\hat{R}e_c = 250\alpha. \tag{5}$$

The subscript c denoting the critical Reynolds number has been used here because below this line there are no disturbances and the flow is stable, while above this line disturbances begin to appear and can grow to more highly disturbed conditions. From a physical viewpoint, increasing α corresponds to a decrease in the time available in one cardiac cycle as compared with the time required for amplification of a disturbance. Equation (5) indicates that under such conditions a higher Reynolds number must be achieved in order for turbulence to develop.

A crude justification for the form of (5) can be developed by applying boundary-layer stability theory to the aortic wall boundary layer. This is done by considering the forward flow in systole to be comparable to that associated with the instantaneous acceleration of flow over a flat plate. The velocity profile in this case is not unlike that of a steady flat-plate boundary layer and the critical Reynolds number criteria for a flat plate based on the boundary-layer thickness δ may be applied as a first approximation, i.e.

$$\hat{R}e_c = (\hat{U}\delta/\nu)_c \simeq 1000. \tag{6}$$

One need then only estimate the boundary-layer thickness. Using Stokes' first problem of an instantaneously accelerated flat plate and taking $t \simeq \frac{1}{4}\omega^{-1}$ as the approximate duration of systole, then, upon substitution, the dependence of the aortic wall boundary-layer thickness on α is predicted to be

$$\delta/R \approx 2/\alpha. \tag{7}$$

A similar result (Nerem 1969) may be obtained from examining Womersley's (1958) solutions or the measured aortic boundary-layer profiles of Ling *et al.* (1968), where only the constant will be different. Furthermore, because of the relatively poor experimental information available on the aortic wall boundary layer, the choice of the constant for (7) is somewhat arbitrary.

However, upon combining (6) with an equation of the form of (7), the dependence of the critical Reynolds number on α may be shown to be

$$\hat{R}e_c = \text{constant} \times \alpha, \tag{8}$$

with the constant of proportionality ranging from 250 to 1000, depending upon the value of the constants is used in (7). The correlation of the data, equation (5), may be seen to be of the same form as (8) but with a constant at the lower end of the range estimated above from boundary-layer theory. This in fact would be expected since the disturbances are generally observed to occur during flow deccleration in systole, and decelerating flows such as this exhibit inflexion points in their velocity profiles and are more unstable than accelerating or steady flows (Shen 1961). This specific point will be looked at in more detail shortly; however, the general agreement of (8) with the data suggests the instability of the aortic wall boundary layer as a plausible explanation for the appearance of the observed disturbances.

Now the measurements reported here have been carried out in the inviscid core of the aortic flow and not in the boundary layer. However, disturbances in the boundary layer may be transmitted to the inviscid core, in this case primarily by sound waves and the associated pressure fluctuations. Of course, the inviscid core flow may also contain disturbances convected along the aorta from the heart. However, the descending aorta data in figure 13 represents primarily conditions where the velocity probe was seeing blood in its second pulse since being ejected from the heart. This in general was true for both highly disturbed, disturbed and undisturbed conditions and thus the blood observed by the probe had already undergone a quiescent diastolic period. Because of this, the development of disturbances in the descending aorta in the present series of experiments is believed to be due to a basic flow instability which occurs anew on each beat.

In figure 14 similar data on the disturbed nature of aortic flow are presented as a function of $\hat{R}e$ and α for the ascending aorta. Again an approximate demarcation line between the undisturbed and the disturbed or highly disturbed points may be drawn with the resulting equation being

$$\hat{R}e_c = 150\alpha. \tag{9}$$

The constant in this case is a factor of two less than for the descending aorta. However, it should be remembered that here the blood is being observed on its

ejection stroke from the heart and thus may already carry appreciable disturbances which might be expected to modify the critical Reynolds number of the wall boundary layer. Reductions of the order of a factor of two in critical Reynolds number are not unreasonable, as was demonstrated in the experiments of Dryden (1936).

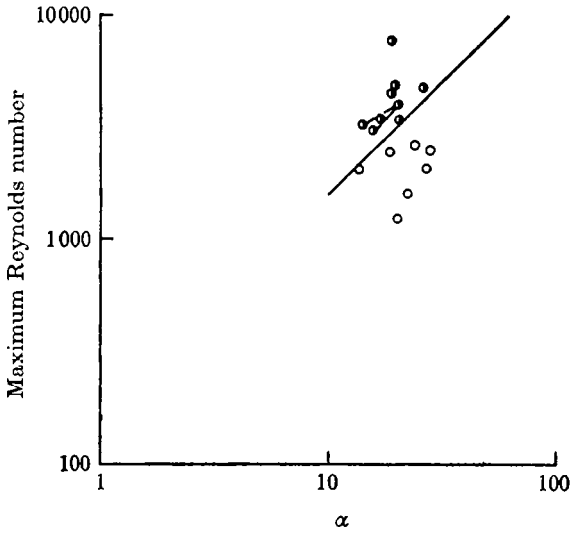

FIGURE 14. Reynolds number and frequency parameter α for the ascending aorta. ——, equation (9); other symbols as in figure 13.

Thus the ascending aorta data presented here in figure 14 are not inconsistent with the descending aorta data of figure 13. Furthermore, the explanation of the data shown in figure 12, which was discussed earlier, may now be elaborated. In this dog both ascending and descending aorta data were obtained under control and isoprenaline infusion conditions. The ascending aorta probe in all cases observed blood during its ejection stroke, while the probe in the descending aorta observed blood during its second stroke. In the control case, the ascending aorta flow was highly disturbed while the descending aorta flow was not. In this case it appears that the probe in the ascending aorta either detected high frequency disturbances coming from the heart itself, or else propagated disturbances triggered in the boundary layer by the lower frequency disturbances commonly associated with flow close to the heart. In the descending aorta, however, the flow was undisturbed in the control case because, for the α of this flow, the Reynolds number $\hat{R}e$ was subcritical. On the other hand, in the isoprenaline infusion case both ascending and descending aorta flows were highly disturbed or turbulent. In this case the change in the nature of the descending aorta flow was due to the sharp increase in $\hat{R}e$ to a supercritical value owing to the isoprenaline.

The stability of the aortic wall boundary layer may be examined in somewhat more detail by considering the effect of velocity profile inflexion during systolic deceleration. This may be done by examining the stability characteristics of the Falkner–Skan velocity profiles (see Schlichting 1968). Each of the profiles in this

family of solutions is characterized by a pressure gradient or acceleration parameter β such that, for $\beta > 0$, the pressure gradient is favourable, corresponding to flow acceleration; for $\beta = 0$, the pressure gradient corresponds to the flat-plate solution and, for $\beta < 0$, the pressure gradient is adverse, corresponding to flow deceleration. In this latter case there will be an inflexion in the velocity profile, the strength of which will increase as β decreases. In figure 15, the present experimental data are compared with Falkner–Skan neutral stability curves

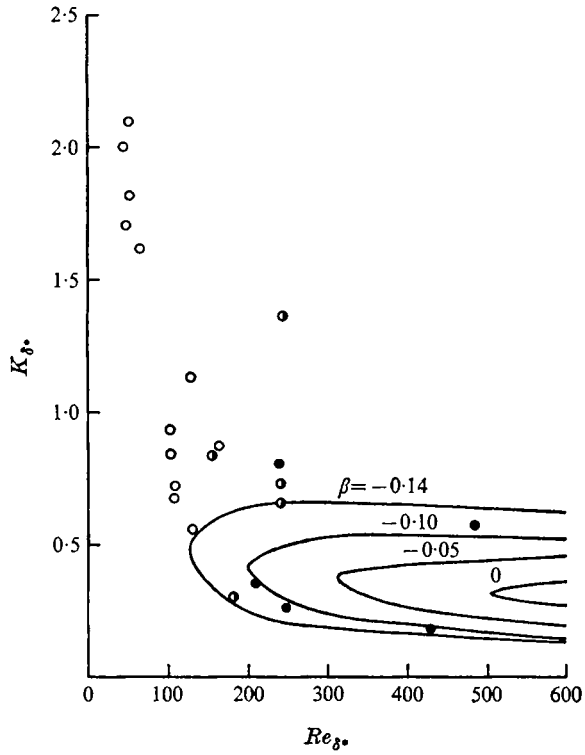

FIGURE 15. Comparison of experimental observations with Falkner–Skan neutral stability curves (from Obremski, Morkovin & Landahl 1969). ○, undisturbed flow; ◑, disturbed flow; ●, highly disturbed flow.

(Obremski *et al.* 1969) corresponding to β values of 0, $-0{\cdot}05$, $-0{\cdot}10$ and $-0{\cdot}14$. The wavenumber K has been based on a disturbance frequency of 125 Hz, which is representative of that observed in these experiments, and the boundary-layer displacement thickness δ^* has been calculated using the results of Stokes' first problem. Re_{δ^*} is the Reynolds number based on peak velocity and the displacement thickness.

In figure 15, the region outside the neutral stability curve corresponds to stable flow, while inside the curve amplification of disturbances will take place. It may also be seen, as would be expected, that the trend in going from the undisturbed data points to the disturbed and highly disturbed points is towards decreased stability. In comparing these data points with the neutral stability curve for $\beta = 0$, the flat-plate case (it should be noted that the shape of the Blasius profile

is quite similar to that resulting from Stokes' first problem), it is clear that even the highly disturbed points lie well into the stable region. However, the highly disturbed data points do follow the neutral stability curve for $\beta = -0{\cdot}10$ very closely and suggest that the idea of an aortic wall boundary-layer instability determined by the velocity profile inflexion is appropriate. It is also of interest to note that, whereas the maximum amplification rate associated with the $\beta = 0$ case is nowhere near sufficient to be consistent with the observations reported here, the amplification rate for an inflected profile with $\beta = -0{\cdot}10$ to $-0{\cdot}14$ is of

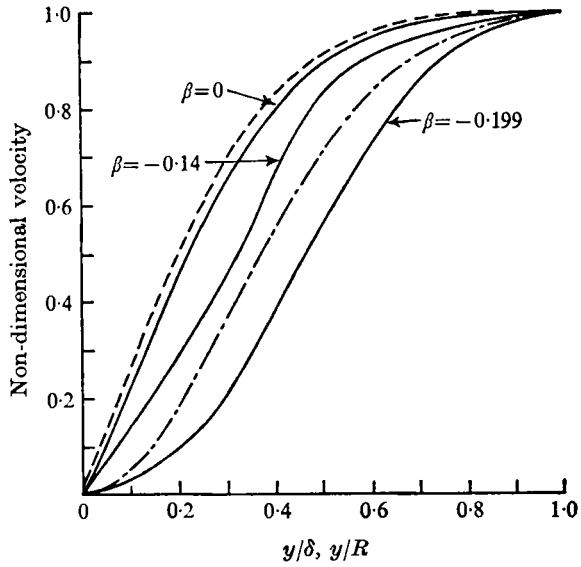

FIGURE 16. Comparison of pulsatile flow velocity profiles (Womersley 1958). – –, $\alpha = 5$, $\omega t = \frac{1}{2}\pi$; —·—, $\alpha = 5$, $\omega t = \frac{3}{4}\pi$; ——, Falkner–Skan velocity profiles (Schlichting 1968) for selected values of β.

the correct order of magnitude. Finally, it should be noted that calculations using the results of Womersley's analysis for $\alpha = 5$ and $\alpha = 10$ suggest that the velocity profiles for a pulsatile flow in the aorta are not unlike those of the Falkner–Skan family. This is shown in figure 16, where Falkner–Skan profiles for $\beta = 0$, $-0{\cdot}14$, $-0{\cdot}199$, in the form of the non-dimensional velocity versus y/δ, are compared with velocity profiles for the case of sinusoidal flow in a rigid tube with $\alpha = 5$. In this latter case, the non-dimensional velocity versus y/R (R = tube radius) is shown for two different times. $\omega t = \frac{1}{2}\pi$ corresponds to peak forward flow, i.e. the equivalent of peak systole, and $\omega t = \frac{3}{4}\pi$ corresponds to a time during the deceleration phase which is 45° later in the cycle. Disturbances (see for example, figure 9) normally appear immediately after peak systole in the experiments and comparison of the profiles in figure 16 suggests that the velocity profile at this time would correspond approximately to a Falkner–Skan profile with β in the range of $-0{\cdot}05$ to $-0{\cdot}10$.

Although this is obviously no proof as to the role of the boundary layer in the generation of the disturbances observed in our experiments, these results are

highly suggestive of the fact that the inflexion of the velocity profile during systolic deceleration is the most important factor. Obviously, such a quasi-steady approach to the stability of the aortic wall boundary layer is an oversimplification. This may equally well be said of the use of the results of Stokes' first problem to evaluate δ^*. Furthermore, there are other possible explanations for the origin of the observed disturbances. These include, as previously noted, disturbances emanating from the heart, convected along the aorta and interacting with each other with no energy being drained from the mean flow but with the disturbance energy cascading into smaller eddies and being associated with higher frequencies. This process might tend to be modified by the presence of an elastic wall through which disturbances can propagate more quickly than by convection. Another possible explanation for the observed disturbances is an instability of the Kelvin–Helmholtz type associated with flow past flexible boundaries. Preliminary calculations by Dr E. H. Ellen (private communication) suggest that this effect is unlikely to be relevant until the mean velocity is several times higher than in these experiments.

It should of course be pointed out that these experiments represent only a preliminary investigation of the nature of flow disturbances and turbulence generation in arteries, though the earlier reported results of Ling *et al.* (1968) and Schultz *et al.* (1969) are in general in agreement with the results in figures 13 and 14. A great deal more needs to be done, particularly regarding the more exact application of stability theory and the laboratory study of the fluid-mechanical aspects of pulsatile flows in conditions comparable to aortic flow. Equally, the aortic flow conditions in conscious animals and man, both when resting and during exercise, require definition. What little data exists (see, e.g. Noble *et al.* 1966) suggests that dogs may normally operate in a state of transitional or turbulent flow. If this were true also in man, it would have considerable clinical importance in terms of arterial wall shear stress, blood mixing and sound production.

This research was aided by grants from the Wates and Nuffield Foundations. R. M. Nerem received support from the Science Research Council and was on leave from the Ohio State University. W. A. Seed received support from St Thomas's Hospital Endowment Fund and the Medical Research Council. N. B. Wood received support from trusts including the Skinners' and Goldsmiths' Companies and Pfizer Ltd. The authors are deeply indebted to Dr T. J. Pedley for his suggestions and for the many discussions into which he entered.

REFERENCES

Atabek, H. B. & Chang, C. C. 1961 Oscillatory flow near the entry of a circular tube. *Z. angew. Math. Phys.* **12**, 185–201.

Barnett, G. O., Mallos, A. J. & Shapiro, A. 1961 Relationship of aortic pressure and diameter in the dog. *J. Appl. Physiol.* **16**, 545–548.

Bellhouse, B. J. 1970 Fluid mechanics of a model mitral valve. *J. Physiol.* **208**, 72–73*P*.

Bellhouse, B. J. & Talbot, L. 1969 Fluid mechanics of the aortic valve. *J. Fluid Mech.* **35**, 721–735.

Dryden, H. L. 1936 Air flow in the boundary layer near a plate. *N.A.C.A. Rep.* no. 562.

Goldstein, S. 1938 *Modern Developments in Fluid Dynamics.* Clarendon.

INOUYE, A. & KOSAKA, H. 1959 A study with the electromagnetic flowmeter of flow patterns in carotid and femoral arteries of rabbits and dogs. *J. Physiol.* **147**, 209–220.

JONES, A. S. 1970 Wall shear in pulsatile flow. *Appl. Math. Preprint University of Queensland*, no. 35,

KUCHAR, N. R. & OSTRACH, S. 1967 Unsteady entrance flows in elastic tubes with application to the vascular system. *Case Western Reserve University Rep.* FTAS/TR-67-25.

LING, S. C., ATABEK, H. B., FRY, D. L., PATEL, D. J. & JANICKI, J. S. 1968 Application of heated-film velocity and shear probes to hemodynamic studies. *Circulation Res.* **23**, 789–801.

MCDONALD, D. A. 1960 *Blood Flow in Arteries.* London: Edward Arnold.

NEREM, R. M. 1969 Fluid-mechanical aspects of blood flow. *Proc. of 8th Int. Symp. on Space Tech. & Sci.* To be published.

NIKURADASE, J. 1934 In *Applied Hydro- and Aerodynamics* (ed. L. Prandtl & O. G. Tietjens). McGraw-Hill.

NOBLE, M. I. M., GABE, I. T., TRENCHARD, D. & GUZ, A. 1967 Blood pressure and flow in the ascending aorta of conscious dogs. *Cardiovascular Res.* **1**, 9–20.

NOBLE, M. I. M., TRENCHARD, D. & GUZ, A. 1966 Measurement and significance of the maximum acceleration of blood from the left ventricle. *Circulation Res.* **19**, 139–147.

OBREMSKI, H. J., MORKOVIN, M. V. & LANDAHL, M. 1969 Portfolio of the stability characteristics of incompressible boundary layers. *AGARDOgraph*, no. 134.

OHLSSON, N.-M. 1962 Left heart and aortic blood flow in the dog. *Acta Radiologica. Suppl.* **213**, 1–80.

SARPKAYA, T. 1966 Experimental determination of the critical Reynolds number for pulsating Poiseuille flow. *Trans. A.S.M.E.* 66-FE-S, 1–10.

SCHLICHTING, H. 1968 *Boundary Layer Theory.* McGraw-Hill.

SCHULTZ, D. L., TUNSTALL PEDOE, D. S., LEE, G. DE J., GUNNING, A. J. & BELLHOUSE, B. J. 1969 Velocity distribution and transition in the arterial system. In *Circulatory and Respiratory Mass Transport. A Ciba Foundation Symposium* (ed. G. E. W. Wolstenholme & J. Knight), pp. 172–199. London: Churchill.

SEED, W. A. 1969 Fabrication of thin-film microcircuits on curved substrates. *J. Sci. Instrum.* **2**, 206.

SEED, W. A. & WOOD, N. B. 1969 An apparatus for calibrating velocity probes in liquids. *J. Sci. Instrum.* **2**, 896–898.

SEED, W. A. & WOOD, N. B. 1970*a* Development and evaluation of a hot-film velocity probe for cardiovascular studies. *Cardiovascular Res.* **4**, 253–263.

SEED, W. A. & WOOD, N. B. 1970*b* Use of a hot-film probe for cardiovascular studies. *J. Sci. Instrum.* **3**, 377–384.

SEED, W. A. & WOOD, N. B. 1971 Velocity patterns in the aorta. *Cardiovascular Res.* **5**, 319–330.

SHEN, S. F. 1961 Some considerations on the laminar stability of time-dependent basic flows. *J. Aerospace Sci.* **28**, 397–417.

VIDAL, R. J. & GOLIAN, T. C. 1967 Heat-transfer measurements with a catalytic flat plate in dissociated oxygen. *A.I.A.A. J.* **5**, 1579–1588.

WOMERSLEY, J. R. 1958 The mathematical analysis of the arterial circulation in a state of oscillatory motion. *Wright Air Development Center, Tech. Rep.* no. WADC-TR-56-614.

WOOD, N. B. 1971 Ph.D. thesis, University of London.

YELLIN, E. L. 1966 Laminar-turbulent transition process in pulsatile flow. *Circulation Res.* **19**, 791–804.

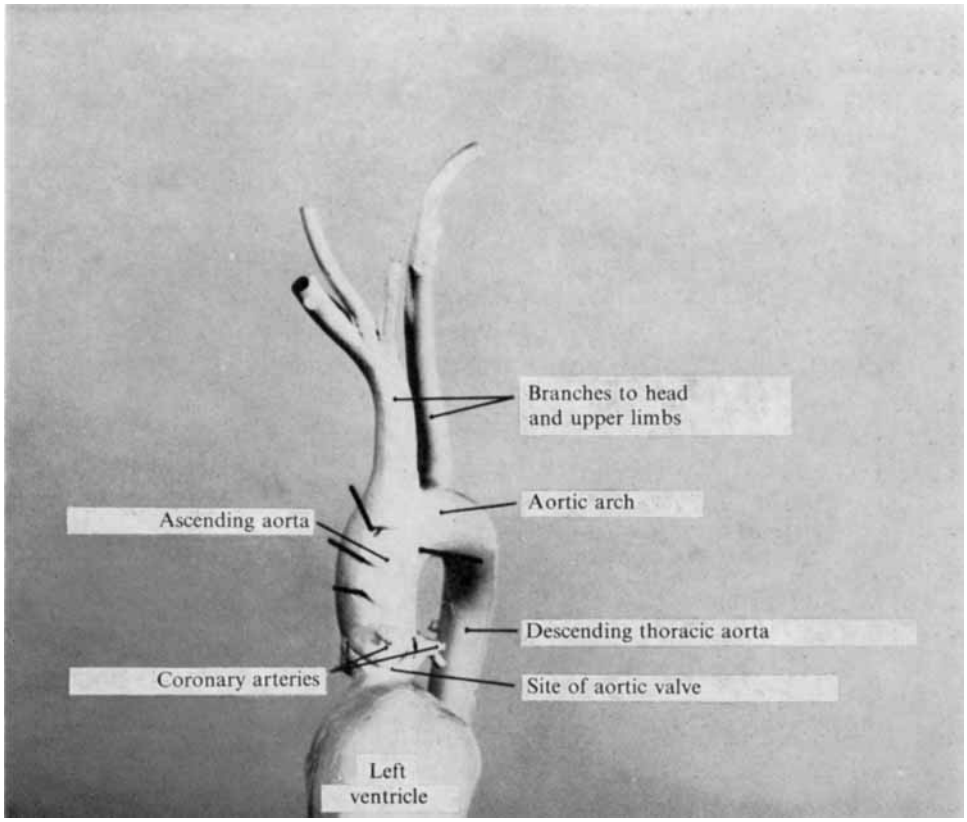

FIGURE 1. Cast of the thoracic aorta of a dog, made by perfusing with liquid resin with normal pressure maintained during hardening. Traverse sites marked with needles.